SCIENTIFIC REPORT - SUMMARY

Stage-3: January– September 2017

Project title: "**Polymer-based materials as sorbents for the enhanced removal of oil spills and dyes from the contaminated waters**"

Project code: **PN-II-RU-TE-2014-4-1266;** Acronym: **POLYSORB**; Contract: no. **95 / 01.10.2015**

OBJECTIVE – II : Preparation and characterization of polymer-based composite materials and their application for the removal of dyes from synthetic wastewaters

Activity II.4 *Modeling and optimization of the adsorption processes*

In this section, the adsorption systems of interest were investigated by the design of experiments (DoE) and response surface methodology (RSM) in order to develop mathematical models useful for optimization of adsorption processes. In this respect, the scientific programs were employed for computations, such as *Design-Expert*, *scilab* and *matlab*.

The design of experiments (DoE) represents a statistical tool usually employed for process investigation by varying the independent factors simultaneously and determining the output variables (responses) of the process. According to RSM and based on collected data (DoE), the empirical models are developed by means of multiple regression method. Generally, a response surface model represents a second-order polynomial equation with interaction terms that can be expressed as [1]:

$$\hat{Y} = b_0 + \sum_{i=1}^{n} b_i x_i + \sum_{i=1}^{n} b_{ii} x_i^2 + \sum_{i<j}^{n} b_{ij} x_i x_j \qquad \text{(II.4.1)}$$

where $\hat{Y}$ denotes the predicted response of the process under investigation; x_i – input variables or independnet factors (coded values); b_0, b_i, b_{ii}, b_{ij} – coefficients of the model (offset, linear, quadratic and interaction terms). The coefficients $\mathbf{b}=\{b_0, b_i, b_{ii}, b_{ij}\}^T$ that represents the model parameters are calculated by means of the multiple regression method as follows [1-2]:

$$\mathbf{b} = \left(\mathbf{X}^T\mathbf{X}\right)^{-1}\mathbf{X}^T\mathbf{Y} \qquad \text{(II.4.2)}$$

where **b** denotes the column-vector of regression coefficients, **X** – design matrix of input variables (coded values), $\mathbf{X}^T$- transposed matrix, and **Y –** column-vector of the response (observed values determined by experimentation).

The first application dealt with modeling of the adsorption process related to Rhodamine-6G dye removal using Ca-Alginate/$NiFe_2O_4$ composite adsorbent. In all experiments the produced composite adsorbents (Ca-Alginate/ $NiFe_2O_4$) as plate-like irregular particles were applied for the removal of the cationic dye (Rhodamine-6G) from aqueous solutions containing 50 mg/L initial dye concentration. The experiments were carried out according to a full factorial design, and the adsorption process was monitored by UV-VIS method (526 nm). Consequently, a multivariate regression model was developed to predict the adsorption capacity (q, mg/g) of materials as a function of controllable factors (i.e. alginate concentration, amount of $NiFe_2O_4$ and $CaCl_2$ concentration). The developed mathematical model in terms of actual variables is given as follows:

$$\hat{q} = 8.3 + 4.51C_1 + 0.18C_2 + 41.7C_3 - 0.046C_1C_2 - 25.1C_1C_3 - 1.44C_2C_3 \qquad \text{(II.4.3)}$$

subject to: $2.0 \leq (C_1 : \text{Alginate}) \leq 3.0$ % w/w; $15 \leq (C_2 : NiFe_2O_4) \leq 25$ % w/w; $0.05 \leq (C_3 : CaCl_2) \leq 0.15$ M

The response surface plot showing the effect of factors on the material's response (i.e. adsorption capacity) is depicted in Fig.2. The model-based optimization enabled to find the optimal composition of the material (i.e., C_1=3% w/w; C_2=15% w/w and C_3=0.05M) that ensured the highest adsorption capacity of q = 19.7 mg/g.

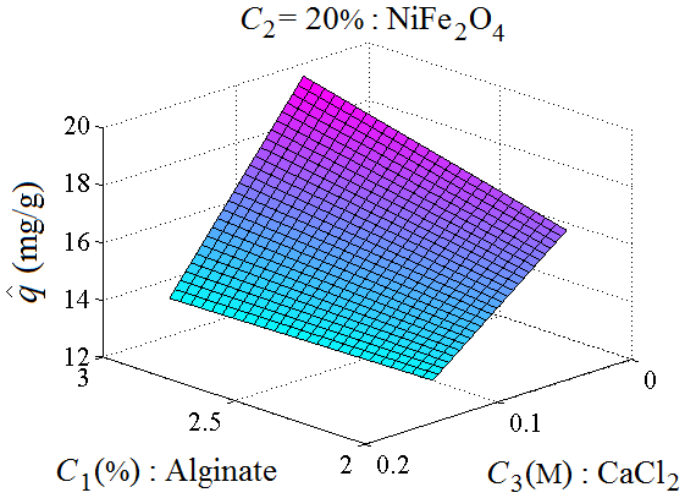

Fig.II.4.1. Response surface plot showing the adsorption capacity (q) of the composite adsorbent (Ca-Alginate/ $NiFe_2O_4$) depending on the factors (C_1: Alginate content) and (C_3: concentration of CaCl2 in the cross-linking bath) at constant dosage of 20% $NiFe_2O_4$.

As shown in **Fig.II.4.1**, higher amount of alginate and lower concentration of $CaCl_2$ is required to develop composite adsorbents with improved efficiency for Rh6G dye uptake. According to the interaction effect between these two factors, the influence of alginate dosage is more pronounced at lower $CaCl_2$ concentration, whereas the effect of $CaCl_2$ concentration is more important at greater amount of alginate.

* * *

The second modeling-optimization application dealt with *Orange II (anionic dye)* adsorption onto $CoFe_{1.98}Sm_{0.02}O_4$@CS-ECH composite adsorbent. In this application, the influence of pH and sorbent dosage (*SD*) factors on the adsorption performance was investigated by using the design of experiments (DoE) and response surface methodology (RSM).

Thus, the synergetic effect of both factors (pH and sorbent dosage, *SD*) was studied with the purpose to improve the adsorption efficiency assessed in term of color removal efficiency, *Y (%*). The considered constant conditions for experimentations were C_0 = 50 mg/L (initial *Orange II* dye concentration); t = 180 min (contact time) and T = 25 ^{o}C (temperature). Following this approach, experimental data were collected according to a central composite design of *rotatable type*, and the data were modeled using Design-Expert 10 software. The developed data-driven mathematical model can be written as:

$$\hat{Y} = b_0 + b_1 \times \mathrm{pH} + b_2 \times SD + b_{11} \times \mathrm{pH}^2 + b_{22} \times SD^2 + b_{12} \times \mathrm{pH} \times SD \qquad \text{(II.4.4)}$$

subjected to (region of experimentation): $3.17 \leq \mathrm{pH} \leq 8.83$; $1.58 \leq SD \leq 4.41$ (g/L)

The final empirical model (Eq. II.4.4) was checked for the adequacy using the analysis of variance (ANOVA) [1]. According to ANOVA outcomes, the model was considered statistically significant and it could be used to explore the design space by simulations.

By using the developed data-driven model (Eq.II.4.4), the response surface plot and was rendered to show the coupling effects of factors (*SD* and pH) on the removal efficiency response *Y*(%) (see **Fig.II.4.2**). According to **Fig II.4.2**, the most significant factor affecting the color removal efficiency is the sorbent dosage (*SD*). Surprisingly, the increment of this factor (*SD* > 2 g/L) resulted in lower values of response (*Y*, %). This might be explained by the fact that for the conditions of *SD*=2g/L the adsorption equilibrium was already established, and higher sorbent dosage (*SD* > 2 g/L) did not yield a better sorption efficiency. This observation suggested an excellent efficiency of the developed adsorbent that can be used even in small amounts, due to a great number of functional

amine groups from chitosan. The second factor, i.e. pH, as well as the interaction effect between both factors *SD* and pH revealed diminished impacts on the adsorption performance.

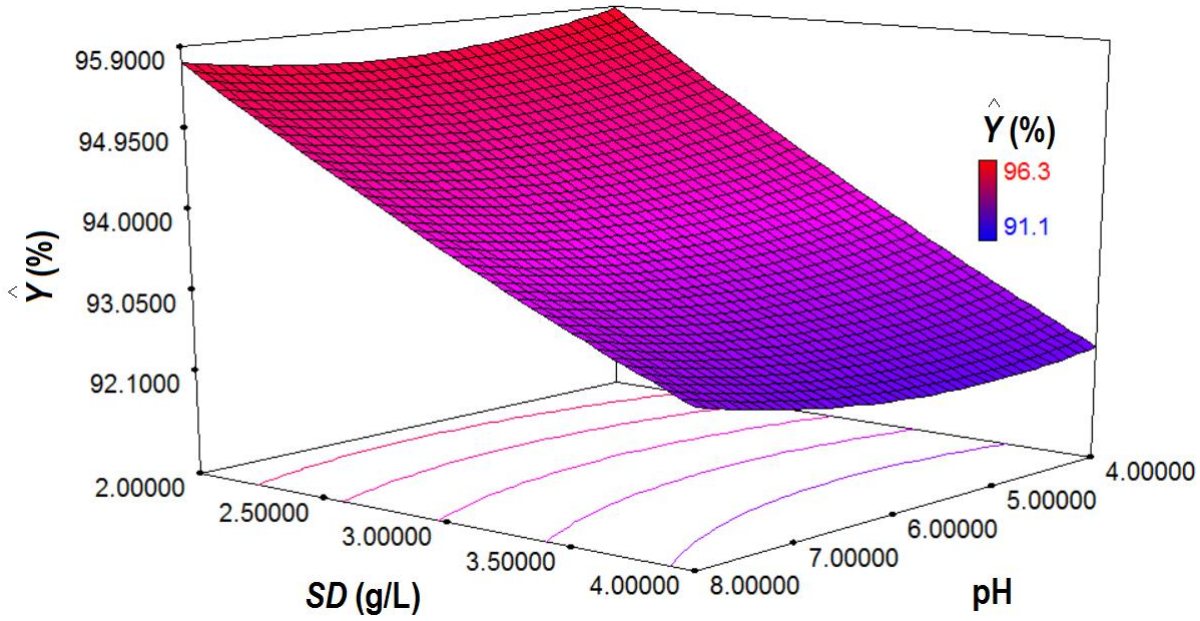

Fig.II.4.2. Response surface showing the coupling effects of pH and *SD* factors on the color removal efficiency *Y* (%); adsorption system: $CoFe_{1.98}Sm_{0.02}O_4$@CS-ECH + *Orange-II dye*.

Model-based optimization was done by stochastic simulation using Monte-Carlo method [3]. The optimal values of factors were determined as pH 5.2 and 1.6 g/L sorbent dosage. In these optimal conditions, the maximal removal efficiency was found to be 96.3% (experimentally observed value).

* * *

The third modeling-optimization application dealt with *Amaranth (anionic dye)* adsorption onto $CoFe_{1.98}Sm_{0.02}O_4$@CS-GA composite adsorbent. In this case, we developed an ***artificial neural network* (ANN)** as a "black-box" model for the prediction of the process performance [2, 4-6]. By using collected data (experimental design) we were able to develop a ***feed-forward* ANN model** trained by a ***back-propagation*** algorithm based on Levenberg-Marquardt method. The architecture (topology) of the feed-forward artificial neural network model (ANN) comprised an input layer with four input variables (*i.e.*, x_1 – pH, x_2 – *SD* (g/L), x_3 – *t* (time, min), x_4 – *T* (^{o}C)), a hidden layer with five processing units with ***logsig*** activation function, and an output layer with one processing unit activated with ***purelin*** transfer function (see **Fig.II.4.3**).

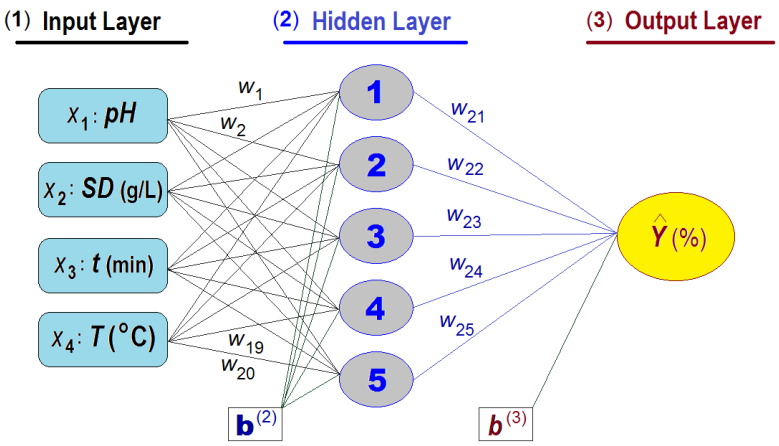

Fig.II.4.3. Feed-forward topology of the developed ANN-model used for prediction of the color removal efficiency related to the adsorption system: $CoFe_{1.98}Sm_{0.02}O_4$@CS-GA + *Amaranth* dye.

The developed ANN model can be written in a general matrix-vector expression as follows:

$$\hat{\mathbf{Y}}(\mathbf{x}) = \mathbf{f}^{(3)}_{purelin}\left(\mathbf{LW}^{(2,3)}\mathbf{f}^{(2)}_{logsig}\left[\mathbf{IW}^{(1,2)}\mathbf{x}+\mathbf{b}^{(2)}\right]+b^{(3)}\right) \quad \text{(II.4.5)}$$

where, **Y** denotes the vector of the output (network predictions), **x** is the vector of the input variables, $\mathbf{f}^{(2)}$ is the vector of ***logsig*** transfer function corresponding to the hidden layer (layer-2), $\mathbf{f}^{(3)}$ is the vector of ***purelin*** transfer function corresponding to the output layer (layer-3), $\mathbf{IW}^{(1,2)}$ is the input weight matrix, $\mathbf{LW}^{(2,3)}$ is the layer weight vector, $\mathbf{b}^{(2)}$ is the bias vector, and $b^{(3)}$ is the bias scalar.

Based on ANN-model (Eq. II.4.5) we developed the predictions maps to reveal the non-linear relationship between input and output variables, as shown (as example) in **Fig.II.4.4**.

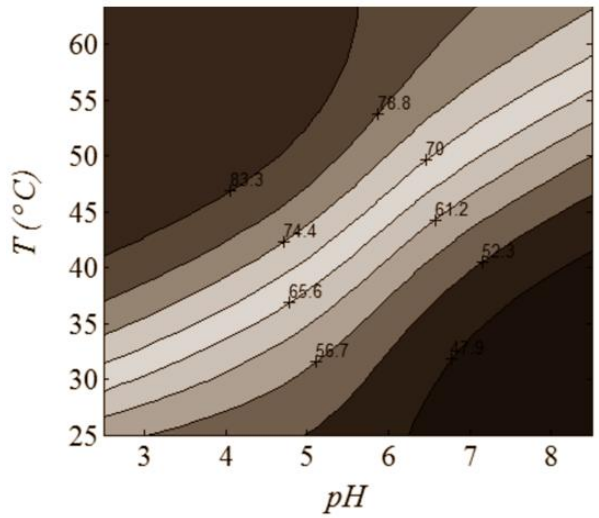

Fig.II.4.4. ANN prediction map showing influences of T(°C) and pH on the output variable Y(%); *i.e.*, color removal efficiency (Y,%) for the adsorption system: $CoFe_{1.98}Sm_{0.02}O_4$@CS-GA + *Amaranth*.

The model-based optimization was performed by coupling the ANN-model with the ***genetic algorithm*** (GenAlg) [6]. Hence, ANN-GenAlg approach enabled to establish the optimal conditions (pH 2.5 and T=65^{o}C) under which the maximum adsorption efficiency of 99.5% was attained.

Activity II.5 *Development of the polymer assisted ultrafiltration process for the removal of dyes from the synthetic wastewaters*

The polymer assisted ultrafiltration (PAUF) is a hybrid adsorption/complexation-membrane separation process that was employed in this study to remove the cationic and anionic dyes from contaminated waters. For the purpose to remove the cationic and anionic dyes from aqueous solutions, polyacrilic acid (PAA, M_w=250 kDa) and polyethyleneimine (PEI, M_w=750 kDa) were used as the binding polymers, respectively. All experiments were carried out in a batch stirred cell and dead-end ultrafiltration mode using the flat sheet polymeric membranes. The experimental ultrafiltration (UF) setup is rendered in **Fig.II.4.5** comprising: an air compressor coupled with a pressure vessel equipped with a manometer and connected to the ultrafiltration stirred-cell of 50 cm^3 capacity. The initial permeate flux J (L/m^2.h) was measured by means of a digital balance.

Fig.II.4.5. Experimental setup employed for the ultrafiltration (UF) experiments.

First, the commercial polymeric membranes were employed for optimization of complexation-ultrafiltration conditions (*i.e.*, pH and polymer/dye ratio). To this end, we used the commercial membranes made of regenerated cellulose of type Ultracel (Merck-Millipore) 30kDa (MWCO). All ultrafiltration experiments were done under stirring (200-300 rpm) at room temperature, and by applying an operating pressure of ***P* = 3 bar**. The determined optimal conditions for polymer-dye

complexation processes disclosed the following ranges of factors pH 6.4 - 6.5, and a ratio polymer-to-dye ranging from 0.8 to 2.1, depending on the nature of the binding polymers and dyes.

Subsequently, our study was focused on preparation of polymer/clay nanocomposite membranes by phase-inverse method [7], using polysulfone (PSf) as the basic polymer. As nanoclay particles, we used the commercial Nanomer I.44P clay (Nanomer® / Sigma-Aldrich), which is a montmorillonite surface modified nanoclay containing 35-45% dimethyl-dialkyl (C14-C18) amine. The nanoclay particles were incorporated as fillers into the membrane matrix to enhance the hydrophilic properties of the membrane as well as its mechanical strength. Also, during the membrane synthesis, poly(ethylene glycol) PEG-400 was added as a porogen agent to increase the porosity of the produced membrane. As solvent we used DMAC (dimethylacetamide), whereas as non-solvent the distilled water was used. The composition of the dope solution was about: 75% DMAC, 17% PSF, 7% PEG-400 and 1% nanoclay. The dope solution was casted on glass plate as films (200 – 250 µm thickness) left for about 10 sec for evaporation and immersed in the coagulation bath. The phase-inversion process occurred immediately with the formation of a solid polymeric membrane with the composition of about 95% PSf and 5% nanoclay. The membrane was washed several times with distilled water to remove solvent traces and afterwards left for drying in the open-air.

The obtained composite membranes (denominated as **M-PSf-C**) were characterized by SEM and AFM (atomic force microscopy) to reveal the materials morphology. **Figure II.4.6** shows the results of SEM (**Fig II.4.6a**) and EDAX (**Fig II.4.6b**) analysis revealing the inclusion of inorganic nanoclay particles in the polysulfone (PSf) matrix of the membrane. Also, the SEM and AFM results disclosed the presence of the opening-pores at the surface the composite membrane M-PSf-C.

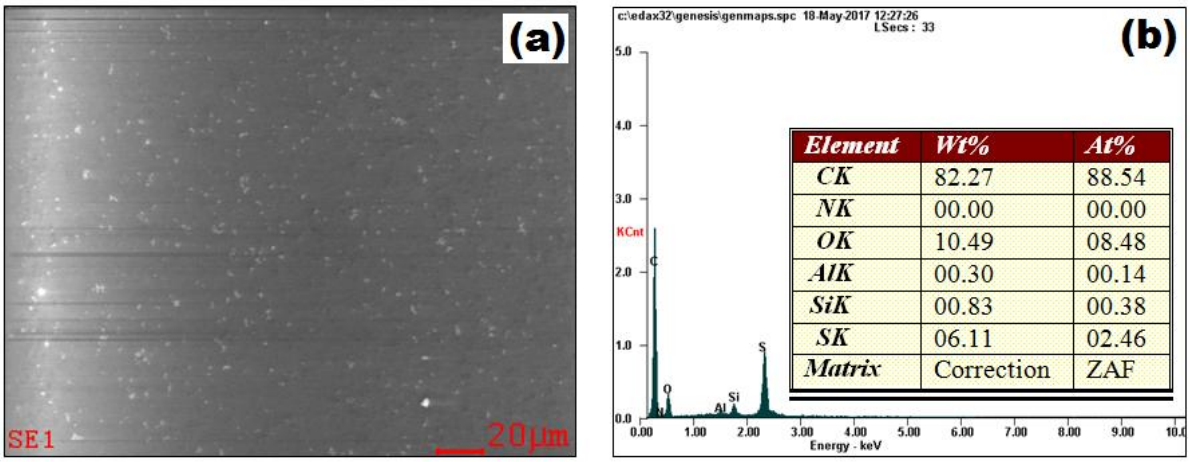

Fig.II.4.6. SEM (a) and EDAX (b) analysis of the produced composite membrane (M-PSf-C).

The produced membranes (M-PSf-C) of various thicknesses were tested for the ultrafiltration of cationic dyes (MB, Rh6G) and anionic dyes (CR, OG-II, AM) in the presence of binding polymers, i.e. polyacrilic acid (PAA, M_w=250 kDa) and polyethyleneimine (PEI, M_w=750 kDa), respectively.

Figure II.4.7 illustrates two digital snapshots showing the ultrafiltration of *Methylene Blue* (MB) dye in the presence of PAA (**Fig.II.4.7A**) and ultrafiltration of *Orange-II* (OG-II) in the presence of PEI (**Fig.II.4.7B**) through the composite porous membrane (M-PSF-C). In addition, the filtrations of other dyes through M-PSf-C membrane were tested, i.e. Rhodamine 6G (Rh6G) in the presence of PAA as well as Congo-Red (CR) and Amaranth (AM) in the presence of PEI. The ultrafiltration performance in terms of color removal efficiency is given in **Table II.4.1** for all investigated systems.

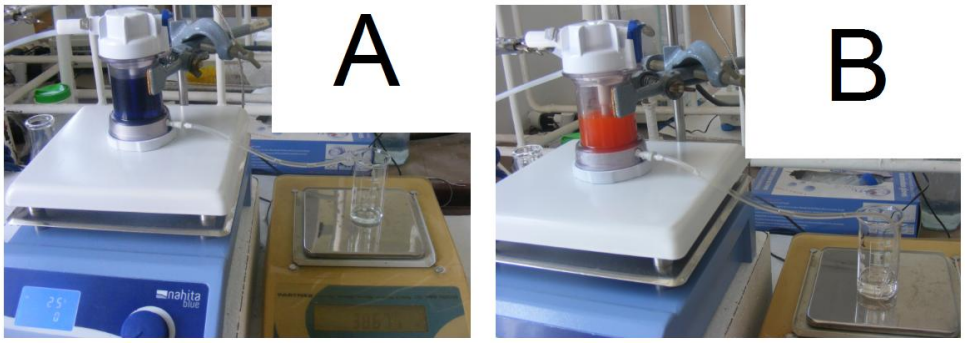

Fig.II.4.7. Digital snapshots showing the ultrafiltration of MB/PAA (**A**) and OG-II/PEI (**B**) complexes through the composite membrane M-PSF-C.

Table II.4.1. Performances of Polymer Assisted Ultrafiltration Process (PAUF) applied for cationic and anionic dyes removal from synthetic wastewaters; ultrafiltration experiments were done through the composite membrane M-PSf-C at room temperature and operating pressure of P=3bar.

M-PSf-C membrane thickness (µm)	Polymer assisted ultrafiltration system (Dye + Polymer)	Initial dye concnentration, (mg/L)	Color removal efficiency, Y (%)
85	Methylene Blue, MB + PAA	50	95.9
125	Methylene Blue, MB + PAA	50	**99.6**
85	Rhodamine-6G, Rh6G + PAA	50	95.5
85	Congo-Red, CR + PEI	100	97.2
125	Congor-Red, CR + PEI	100	**99.2**
85	Orange-II, OG-II + PEI	100	**99.5**
85	Amaranth, AM + PEI	100	87.8

According to data summarized in **Table II.4.1**, the produced membrane (M-PSf-C) disclosed high selectivity for the efficient removal of *Orange-II*, *Methylene Blue* and *Congo-Red* dyes, yielding color removal efficiencies greater than 99%. The lowest color removal efficiency (87.8%) was observed only for the case of *Amaranth* dye filtration in the presence of PEI.

Figure II.4.8 shows the superficial aspects of the spent membranes (M-PSf-C) after the ultrafiltration of dyes. These images pointed out the retention/concentration of dye-polymer aggregates ("cake deposition") onto the solid surfaces of membranes of M-PSf-C type. According to **Figure II.4.8**, the greatest retention density was observed for the case of *Orange-II* (OG-II) dye removal in the presence of PEI; herein the OG-II/PEI aggregates were concentrated almost uniformly onto the entire surface of membrane (see **Fig.II.4.8-5**). In turn, the lowest retention density was observed for the case of Amaranth dye removal assisted by PEI (**Fig.II.4.8-6**). These findings derived from digital images analysis are in good agreement with data reported in **Table II.4.1**.

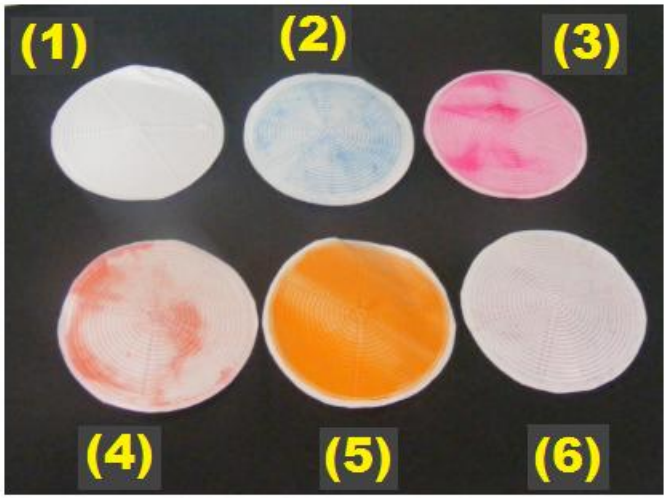

Figure II.4.8. Superficial aspects of spent composite membranes (M-PSf-C) after polymer assisted ultrafiltration of dyes: (**1**) - initial/pristine M-PSf-C membrane; (**2**) - spent membrane after retention of MB-dye/PAA aggregates; (**3**)- spent membrane after retention of Rh6G-dye/PAA aggregates; (**4**)- spent membrane after retention of CR-dye/PEI aggregates; (**5**)- spent membrane after retention of OG-II-dye/PEI aggregates (**6**)- spent membrane after retention of AM-dye/PEI aggregates;

* * *

To reveal the insights of molecular interaction between organic dyes and binding polymers the molecular modeling simulations were carried out. To this end, the molecular modeling software packages were employed such as HyperChem and YASARA-Structure. **Figure II.4.9** shows the optimized molecular structures and electrostatic potentials calculated according to PM3 semi-empirical molecular orbital theory for *Congo-Red* dye (**Fig.II.4.9A**) and *Methylene Blue* dye (**Fig.II.4.9B**). Note that, the electrostatic potential maps around dye molecules indicate the sites of electrophilic and nucleofilic attacks disclosing in fact the sites of interactions with binding polymers. According to **Fig.II.4.9A**, the optimal geometry of *Congo-Red* (CR) molecule suggested an asymmetrical positioning of the anionic moieties ($-SO_3^-$), which induce a negative electrostatic potential in the vicinity of these functional groups. In turn, the optimized molecular structure of *Methylene Blue* (MB) dye (**Fig.II.4.9B**), indicated almost a positive electrostatic potential around this molecule.

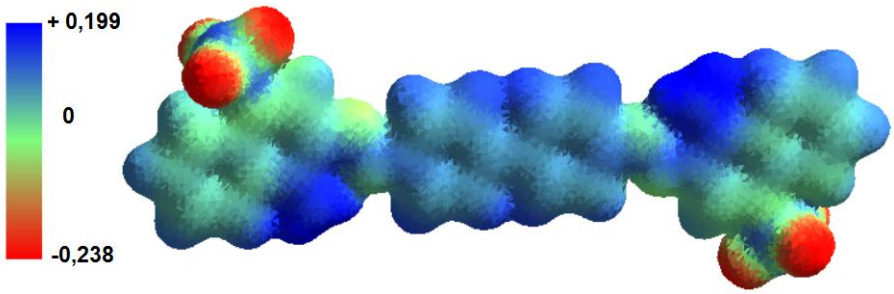

(**A**)

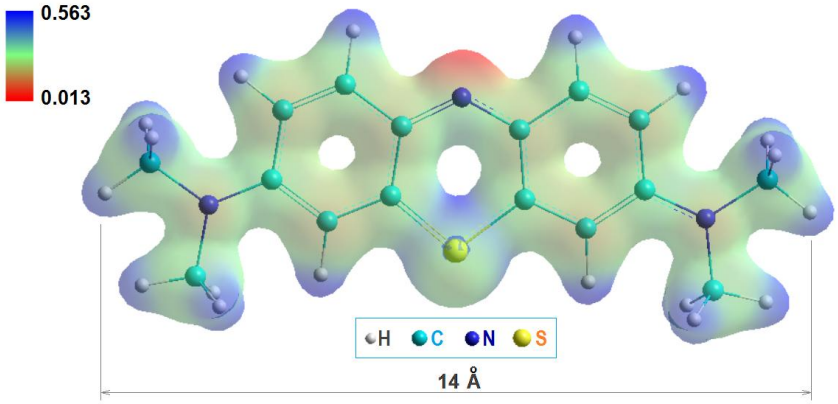

(**B**)

Fig.II.4.9. Optimized molecular structures and electrostatic potential of *Congo-Red dye* (**A**) and *Methylene Blue dye* (**B**); computations done at the level of PM3 molecular orbital theory.

In addition, the intermolecular interactions between CR-dye and PEI as well as between MB-dye and PAA were investigated by molecular docking (AutoDock VINA method [8]) and

molecular dynamics simulations using YASARA-Structure software package [9]. According to these computational results, the CR-PEI aggregates were stabilized by electrostatic and hydrofobic (van-der-Waals) interactions as well as by hydrogen-bonds (H-bonds) formation. For this case, the binding energy (CR-PEI) was equal to E_b = - 4.23 kcal/mol. In turn, the interactions between MB-dye and PAA were based only on electrostatic and hydrofobic interactions without formation of H-bonds. For this system (MB-PAA), the binding energy was higher (E_b = - 3.52 kcal/mol) disclosing a lower stability of MB-PAA aggregates comparing with CR-PEI ones.

Conclusions

In the final stage of the project we were able to perform modeling and optimization of the investigated adsorption processes by using design of experiments, response surface methodology, statistical validation and artificial neural networks. The model-based optimization approach enabled to establish the optimal conditions that ensured the maximal adsorption performances in terms of color removal efficiencies (>96%).

Likewise, in the frame of this project it was developed a polymer assisted ultrafiltration (PAUF) system employed for the removal of organic dyes from the synthetic wastewaters. In this line, the composite membranes based on polysulfone polymer (PSf) and nanoclay particles were synthesized using the phase-inversion method. The produced membrane (M-PSf-C) disclosed high efficiencies (>99%) for the removal of Orange-II, Methylene Blue and Congo-Red dyes from aqueous solutions in the presence of PEI and PAA binding polymers.

By using molecular modeling tools (*i.e.*, electrostatic potential mapping, molecular docking and molecular dynamics) the interactions between dyes and binding polymers were revealed pointing out the existing of electrostatic, hydrophobic and hydrogen-bond-formation interactions.

References

[1] M. Bezerra, et al., *Talanta* **76** (2008) 965-977.
[2] M. Khayet, C. Cojocaru, M. Essalhi, *J. Membr. Sci*. **368** (2011) 202-214.
[3] C. Cojocaru, et al., *J. Taiwan Inst. Chem. Eng*. **70** (2017) 267-281.
[4] M. Khayet, C. Cojocaru, *Sep. Purif. Technol*. **86** (2012) 171-182.
[5] M. Khayet, C. Cojocaru, *Desalination* **308** (2013) 102-110.
[6] N. Marchitan, C. Cojocaru, A. Mereuta, et al., *Sep. Purif. Technol*. **75** (2010) 273-285.
[7] Y. Ma, et al., *Desalination* **286** (2012) 131-137.
[8] O. Trott, A.J. Olson, *J. Comput. Chem*. **31** (2010) 455-461.
[9] E. Krieger, et al., *Proteins* **47** (2002) 393-402.